Quantification of Malignant Breast Cancer Cell MDA-MB-231 Transmigration across Brain and Lung Microvascular Endothelium

Jie Fan and **Bingmei M. Fu**[*]

Department of Biomedical Engineering, The City College of the City University of New York, 160 Convent Ave, New York, NY 10031, USA

Abstract

Tumor cell extravasation through the endothelial barrier forming the microvessel wall is a crucial step during tumor metastasis. However, where, how and how fast tumor cells transmigrate through endothelial barriers remain unclear. Using an in vitro transwell model, we performed a transmigration assay of malignant breast tumor cells (MDA-MB-231) through brain and lung microvascular endothelial monolayers under control and pathological conditions. The locations and rates of tumor cell transmigration as well as the changes in the structural components (integrity) of endothelial monolayers were quantified by confocal microscopy. Endothelial monolayer permeability to albumin $P^{albumin}$ was also quantified under the same conditions. We found that about 98% of transmigration occurred at the joints of endothelial cells instead of cell bodies; tumor cell adhesion and transmigration degraded endothelial surface glycocalyx and disrupted endothelial junction proteins, consequently increased $P^{albumin}$; more tumor cells adhered to and transmigrated through the endothelial monolayer with higher $P^{albumin}$; $P^{albumin}$ and tumor transmigration were increased by vascular endothelial growth factor (VEGF), a representative of cytokines, and lipopolysaccharides (LPS), a typical systemic inflammatory factor, but reduced by adenosine 3′, 5′-cyclic monophosphate (cAMP). These results suggest that reinforcing endothelial structural integrity is an effective approach for inhibiting tumor extravasation.

Keywords

Transmigration locations; Transmigration rates; Endothelial surface glycocalyx; Endothelial junctions; Endothelial solute permeability

Introduction

Tumor cell (TC) extravasation from the blood microcirculation to a distant organ is a crucial step during metastasis [51]. Organ-specific colonization is a key feature of most metastatic tumor cells [22, 40]. Breast cancer cells such as MDA-MB-231 have been known to extravasate preferentially into the lungs and brain [18, 39]. However, where, how and how fast MDA-MB-231 cells transmigrate through these organ-specific endothelial barriers remain unclear.

[*]Corresponding author, (212)-650-7531, (212)-650-6727 (fax), ; Email: fu@ccny.cuny.edu

To search for effective anti-metastatic therapies, many in vivo, ex vivo and in vitro studies have been conducted to understand specific molecular mechanisms by which TCs interact with endothelial cells (ECs) lining the microvessel wall for the adhesion and extravasation [2, 5, 6, 11, 12, 17, 19, 26, 27, 28, 33, 34, 35, 47, 48, 50, 52, 55]. In addition to specific cell adhesion molecules on the TCs and endothelium, endothelial barrier integrity, including inter-endothelial junction proteins (ZO-1, VE-cadherin) and endothelial surface glycocalyx (ESG), is another determinant for TC adhesion and extravasation. ESG is a layer of membrane-bound macromolecules comprised of proteoglycans and glycosaminoglycans (GAGs), which coats luminal surface of blood vessels and plays an important role in regulating vascular permeability, attenuating interactions between circulating cells and ECs, as well as sensing the hydrodynamic changes in the blood flow [14, 15, 16, 24, 38, 42, 43, 53]. Lee et al. [35] found that TC secretion, vascular endothelial growth factor (VEGF), increases MDA-MB-231 cell adhesion and transmigration across the brain microvascular EC monolayer by enhancing monolayer permeability. Similar phenomenon was observed in vivo in individually perfused rat mesenteric microvessels [48]. Fan et al. [19] further reported that VEGF disrupted EC junction proteins, enabling the exposure of underlying basement membrane and increasing the adhesion of TCs to the interendothelial junctions. Weis et al. [59] found that VEGF-mediated Src activity damaged EC barriers in lung endothelium to potentiate tumor cell extravasation and metastasis in a mouse model. In an in vivo study, Cai et al. [8] revealed that MDA-MB-231 cell adhesion to a normal post-capillary venule degrades its ESG.

Many previous studies investigated TC adhesion to microvessel walls as the initial step for extravasation [30, 37, 60]. Using an in vitro real-time model, Heyder et al. [31] demonstrated that invasive human bladder carcinoma cell line T24 irreversibly damages the ECs by inducing apoptosis at the site of TC infiltration. Employing a microfluidic platform, Chen et al. [10] found no disruption to EC junctions after completion of MDA-MB-231 transmigration. Most recently, Joen et al. [32] developed an organ-specific 3D microfluidic model to elucidate the effects of microenvironments on the extravasation of MDA-MB-231 cells and they found that the leakiest environment gave rise to the lowest extravasation rate. In terms of TC adhesion and transmigration locations, previous studies reported that TCs can transmigrate through both the para- and trans-EC pathways [3, 20, 29, 30, 56, 59].

To reconcile above various findings and to quantitatively investigate where, how and how fast tumor cells transmigrate through endothelial barriers, we employed a transwell system to quantify adhesion and transmigration of MDA-MB-231 cells across brain and lung microvascular endothelial monolayers and to quantify endothelial permeability and its structural integrity under the same conditions. This is the first step in finding the underlying mechanism by which TCs transmigrate through the microvessel wall.

Lipopolysaccharide (LPS), a component of the outer membrane of gram-negative bacteria, is a pro-inflammatory agent which can compromise vascular wall integrity [25, 41, 54]. LPS can also increase the adhesion of breast cancer cells to endothelium by directly or indirectly activating ECs [9]. In contrast, adenosine 3′, 5′-cyclic monophosphate (cAMP) can prevent capillary leakiness by LPS-induced systemic inflammation [44]. In addition to VEGF, we used

LPS and cAMP to simulate pathological (e.g. sepsis) and therapeutic (anti-inflammation) conditions and investigated their roles in tumor transmigration.

Materials and methods

Reagents and solutions

Mammalian Ringer solution with 10 mg/ml BSA (1% BSA) (Sigma, A4378) (Ringer-BSA, PH=7.4) was used in both the transmigration assay and permeability measurement [19]. All chemicals in the Ringer solutions, FITC-labeled BSA (MW~67kD, A9771), 8-bromo-adenosine 3′, 5′-cyclic monophosphate (cAMP) and lipopolysaccharides (LPS) were purchased from Sigma-Aldrich (St. Louis, MO). PBS was from Mediatech Inc (Manassas, VA), 4′, 6-diamidino-2-phenylindole (DAPI) from Invitrogen (Carlsbad, CA) and human recombinant VEGF (VEGF$_{165}$) from Peprotech (Rocky Hill, NJ). *F. heparinum* Heparinase III (IBEX, Canada) is selectively active only towards heparan sulfate. 50 mU/mL Heparinase III was used to digest the ESG [8].

Cell culture

Human breast carcinoma cells (MDA-MB-231) and mouse brain microvascular endothelial cells (bEnd3) from ATCC (Manassas, VA) were cultured in Dulbecco's Modified Eagle's Medium/Nutrient Mixture F-12 Ham (DMEM/F-12), 2 mM L-glutamine, and 100 U/mL penicillin and 1 mg/mL streptomycin, all from Sigma-Aldrich, supplemented with 10% fetal bovine serum (FBS, Atlanta Biologicals, Flowery Branch, GA), Rat lung microvascular endothelial cells (RLMECs, VEC Technologies, Rensselaer, NY) were cultured in MCDB-131 complete medium from the same company. All the cells were incubated in the humidified atmosphere with 5% CO_2 at 37 °C.

Transmigration assay

The bEnd3 cells or RLMECs were detached from the culture plates with trypsin-EDTA solution and seeded at 600 cells/mm^2 on the 50 μg/mL fibronectin (Sigma-Aldrich) coated transwell insert with 8 μm pores in a transwell system (BD Labware, Franklin Lakes, NJ), and cultured for 4 d until confluent [19, 36]. MDA-MB-231 cells (TCs hereafter), labeled with Cell Tracker Red (Life Technologies, Grand Island, NY) [8], were added onto the upper chamber of the transwell at a density of 600 cells/mm^2. At 4 h, the non-adherent TCs were washed away and the adherent TCs and EC monolayers in some transwell filters were cultured further to 6 and 8 h. The adherent, transmigrating and transmigrated TCs along with the EC monolayers were fixed with 3.7% paraformaldehyde at 4, 6, and 8 h. For VEGF and LPS treatment groups, 1 nM of VEGF or 5 μg/mL of LPS was presented in the Ringer-BSA in both upper and lower chambers since the TC seeding; for cAMP treatment groups, the EC monolayers were pre-treated for 2 h with 4 mM of cAMP before adding the TCs. cAMP was present in the upper and bottom chambers during entire tumor migration processes. The viability rate was > 95% for both ECs and TCs after 8h incubation under all the conditions.

Immunostaining

Staining of the EC junction proteins—To determine the adhesion and transmigration locations of TCs to EC monolayers, the above fixed samples were first permeabilized with

0.2% Triton X-100 (Sigma-Aldrich), blocked with 10% normal goat serum (NGS, Jackson ImmunoResearch, West Grove, PA) in 0.1% Triton X-100 for 1 h, and incubated overnight with the rabbit anti-ZO-1 (1:200, Life Technologies, Grand Island, NY), followed by Alexa Fluor (AF) 488 conjugated goat anti-rabbit IgG (1:500, Life Technologies) to label the EC junctions. The cell nuclei were stained with 4, 6-Diamidino-2-Phenylindole, Dihydrochloride (DAPI, Life Technologies).

Staining of the EC surface glycocalyx (ESG)—The EC monolayers along with the adherent TCs were fixed with 2% paraformaldehyde with 0.1% Glutaraldehyde, blocked with 2% NGS, and incubated with mouse anti-heparan sulfate 10e4 (1:100, Amsbio, Cambridge, MA) at 4 °C overnight, followed by an AF488 conjugated goat anti-mouse IgG (1:200, Jackson ImmunoResearch, West Grove, PA). Heparan sulfate (HS) is the most abundant GAG in the ESG [24].

Confocal microscopy and image analysis

Confocal microscopy—The transmigration samples were cut off from the transwell filter, spread in between a glass slide and a coverslip, mounted and imaged with Zeiss LSM 710 laser scanning confocal microscope with an oil objective lens (63x/1.4, Zeiss). Ten fields of ~135×135 μm^2 at a resolution of 1024×1024 were randomly chosen for each sample, and captured as a z-stack of thickness 40 μm with a z-step of 0.32 μm for three channels (Cell Tracker Red, AF488, DAPI). For ESG imaging, five fields of ~135×135 μm^2 at a resolution of 1024×1024 were randomly chosen for each sample, and captured as a z-stack of thickness 12 μm with a z-step of 0.32 μm for these three channels. All collected images were analyzed using NIH Image J.

Tumor adhesion/transmigration analysis—TCs were identified as adhesion (AD), transmigrating (TMing), or transmigrated (TMed) phase during the extravasation. TMing phase was further categorized as transmigrating through the bi-joints, or tri-joints of ECs and through EC bodies.

Quantification of EC junction proteins—The intensity profile of ZO-1 staining was plotted along a 3 μm long line perpendicularly to the EC border at the sites with adherent and transmigrating TCs, as well as without TCs. Kurtosis analysis was applied for the intensity distribution profiles under different conditions.

Quantification of EC ESG—The intensity of HS staining from the projection images of z-stack were averaged for the regions of interest (ROIs) with and without adherent TCs to quantify ESG. For ESG degradation, the bEnd3 monolayer was pretreated for 1 h with 50 mU/mL heparinase III before quantification.

Permeability measurement

When EC monolayers became confluent, TCs (600 cells/mm^2) were added to the upper chamber of the Transwell filter. After 4 h incubation, the non-adherent TCs were washed away for each sample and some samples were further incubated to 6 and 8 h. For the control groups, no TCs were added to the EC monolayers. The permeability of EC monolayers with

and without TCs was measured at 4, 6, and 8 h. Briefly, at each time point, the 8 μM FITC-BSA in 1% BSA Ringer was added to the upper chamber of the transwell filter while 1% BSA Ringer was added to the bottom chamber; every 30 min in 90 min, 50 μL of the solution mixed with FITC-BSA diffusing from the upper chamber was collected from the bottom chamber and immediately replaced by the same amount of 1% BSA Ringer. The concentration of FITC-BSA in the collected solution was determined by the plate reader (Bio-Tek, Winooski, VT) with the Ex/Em wavelengths of 485/535 nm. The permeability of

the EC monolayer to FITC-BSA was calculated as $P = \frac{\Delta C/\Delta t}{C_0} \cdot \frac{V}{A}$, where $\Delta C/\Delta t$ is the increase rate of FITC-BSA concentration in the bottom chamber during the time interval Δt, C_0 is the FITC-BSA concentration in the upper chamber (assumed to be constant since the amount of FITC-BSA diffused to the bottom chamber was less than 1% of that in the upper chamber during the measurement period for the control and less than 7.1% for the most permeable case in the current study), V is the solution volume in the bottom chamber which is 1.5 mL, and A is the surface area of the filter, which is 1.12 cm^2. The solution volume in the upper chamber is 0.5 mL. For the treatment groups, 1 nM VEGF or 5 μg/mL LPS was added in the top and bottom chambers from the beginning; for cAMP treatment groups, the EC monolayers were pretreated for 2 h with 4 mM cAMP in both chambers before adding the TCs onto the upper chamber.

Data Analysis

Data were presented as mean ± SE, unless indicated otherwise. Statistical analysis was performed by a two-way (time and different treatments) ANOVA using Sigma Plot 11.2 from Systat Software Inc. (San Jose, CA). Kurtosis analysis was used to compare the distribution profiles under different conditions. A level of $p < 0.05$ was considered a significant difference in all experiments. n = 3 samples at each time point for each treatment.

Results

Tumor cells were identified as adhesion (AD), transmigrating (TMing), or transmigrated (TMed) phase during the extravasation. Figure 1 demonstrates each phase. Same as our previous study in Fan et al.[19], most of the TC adhesion occurred at EC joints (Fig. 2A). TMing phase was further categorized as transmigrating through EC bodies (Fig. 2B), the bi-joints (Fig. 2C), and tri-joints of ECs (Fig. 2D). A transmigrated TC was shown in Fig. 2E.

Tumor cells prefer to transmigrate across the endothelial monolayer through inter-endothelial junctions

The transmigration study shows that out of 121 transmigrating TCs across the bEnd3 monolayer, 65% were through the tri-cellular joint, 33% through the bi-cellular joints and only 2% through the EC body. Similarly, out of 223 transmigrating TCs across the RLMEC monolayer, 63% were through the tri-cellular joint, 35% through the bi-cellular joints and only 2% through the EC body (Fig. 2F).

More tumor cells adhere to and transmigrate across the endothelial monolayer with higher permeability

Figures 2G, H show the number of adherent (Fig. 2A), transmigrating (Fig. 2B-D) and transmigrated (Fig. 2E) TCs at 4, 6 and 8 h, respectively, for the bEnd3 and RLMEC monolayers. Since the total numbers of TCs were the same at different time, the increase in the number of the transmigrating and transmigrated TCs was the same as the decrease in the number of the adherent TCs. At initial transmigration measurement at 4 h, there were 33% more TCs in the RLMEC monolayer (~553 cells/mm^2) than those in the bEnd3 monolayer (~415 cells/mm^2) although the seeding TCs (600 cells/mm^2) were the same. At 4, 6 and 8 h, the percentage of the adherent tumor cells that migrated through was 4.0%, 14.6% and 19.2% for the RLMEC monolayer, and 1.2%, 10.7% and 20.0% for the bEnd3 monolayer, respectively. From Figs 2G, H, even at 8 h, there were still ~57% and 54% adherent TCs for bEnd3 and RLMEC monolayers, respectively. This means that some TCs must take longer than 8 h to accomplish the transmigration or not all of the adherent TCs would cross the EC monolayers. If we define the number of the effective transmigrated TCs as the number of the transmigrated TCs (Fig. 2E,G,H) plus half the number of the transmigrating TCs (Fig. 2B-D,G,H), Fig. 2I demonstrates that although at 4 h, the number of effective transmigrated TCs across the RLMEC monolayer was more than 3 times that across the bEnd3 monolayer, the effective transmigration rate, ~25 cells/mm^2/h was similar for both monolayers between 4 and 8 h. To understand this, we measured the permeability of monolayers to BSA (P) in the presence and absence of TCs. The results are shown in Figs. 2J, K. In the absence of TCs, P of both monolayers did not change with time but P of the RLMEC monolayer was ~6.7 fold that of the bEnd3 monolayer. In the presence of TCs, P of both monolayers increased greatly. Compared to their respective P in the absence of TCs, P in the presence of TCs increased to 2.4, 2.8 and 5.8 fold for the bEnd3 monolayer, and to 2.7, 4.0 and 5.2 fold for the RLMEC monolayer at 4, 6 and 8 h. The increased P strongly correlated with the increased number of effective transmigrated TCs, which was also plotted in Figs. 2J, K.

Tumor cell adhesion and transmigration degrade endothelial surface glycocalyx and disrupt endothelial junctions

Since P of an EC monolayer is determined by its structural components, e.g. endothelial surface glycocalyx (ESG) and endothelial junction proteins (ZO-1, VE-cadherin), the increased P may be caused by degrading ESG and disrupting EC junctions during TC adhesion and transmigration. To test this hypothesis, we did immunolabeling of heparan sulfate (HS), the most abundant GAG in ESG in the absence (control, Fig. 3A) and presence (Fig. 3B) of TCs. After 1h TC adhesion, the intensity of AF488-anti-HS reduced to 40% and 33% of their controls in the regions with adherent TCs, respectively, for the bEnd3 and RLMEC monolayers. The regions without TC adhesion in the same sample in the presence of TCs also had significantly decreased HS intensity from the control, 56% and 41%, respectively, for the bEnd3 and RLMEC monolayers (Fig. 3C). These values were higher than those in the regions with adherent TCs but not significant (p > 0.2). One possible explanation for this is that tumor secretions such as VEGF [21], heparinase and hyaluronidase [57], which can diffuse to the regions without adherent tumor cells and degrade the ESG. Along a 3 μm line perpendicular to the EC junction, the intensity of ZO-1 was

measured for the EC junctions without TCs (Fig. 3D), with adherent TCs (Fig. 3E) and with transmigrating TCs (Fig. 3F). Kurtosis analysis was used to test if the intensity profiles of ZO-1 are different from each other [1]. Since there were no significant differences in the intensity profiles at 4, 6, and 8 h for each case, the intensity profiles shown in Figs. 3G (for bEnd3 monolayer) and **3H** (for RLMEC monolayer) were then the averaged values over 4, 6 and 8 h under each circumstance. The EC junctions without TCs had the highest intensity of ZO-1; the junctions with adherent TCs had less ZO-1 and those with transmigrating TCs had none. These results indicate that TC adhesion partially and transmigration completely disrupts the EC junctions.

Effects of VEGF and LPS on permeability of endothelial monolayers and tumor cell transmigration

To investigate TC transmigration under pathological conditions, we performed the permeability measurement of EC monolayers and TC transmigration assay under the treatment of VEGF, a representative of cytokines, and LPS, a representative of inflammatory factors. Figures 4A, B show the permeability of bEnd3 monolayers to BSA (P) under control and the treatment of VEGF and LPS in the absence and presence of TCs, respectively; Figs. 4D, E show those for RLMEC monolayers. In the absence of TCs, both 1 nM VEGF and 5 μg/mL LPS increased P with more increase under LPS treatments, but the increase did not change with time. We chose 1 nM VEGF because it represents the secretion level of tumor cells observed after prolonged incubation [19]; and it was shown to be an optimal dose that significantly increased tumor cell adhesion and endothelial permeability both in vitro and in vivo [35, 48]. 5 μg/ml LPS was an optimal concentration in the blood during systemic inflammation [25]. In the presence of TCs, P increased with time under control and VEGF and LPS treatments; at 8 h, P became the same under these three conditions for bEnd3 monolayers. This result indicates that the disruptions in the EC integrity by the TC adhesion and transmigration are more serious than those by VEGF and LPS. Figures 4 C, F demonstrate the number of effective transmigrated TCs under control and VEGF and LPS treatments for bEnd3 and RLMEC monolayers, respectively. LPS enhanced TC transmigration across the bEnd3 monolayer to 4.9, 2.6 and 2.1 fold, and VEGF to 2.8, 1.8 and 1.3 fold of those under control at 4, 6 and 8 h; at the same time points, both LPS and VEGF enhanced TC transmigration across the RLMEC monolayer to 2.3, 1.6 and 1.5 fold of those under control.

cAMP can reinforce endothelial junctions and reduce permeability of endothelial monolayers and tumor cell transmigration

To examine if reinforcement of EC junctions inhibits TC transmigration under control and pathological conditions, we pretreated bEnd3 monolayers with cAMP, which was previously shown to increase EC junction integrity [1, 15, 23, 45]. Figure 5A demonstrates that compared to the control in the absence of TCs, pretreatment of bEnd3 monolayers with 4 mM cAMP alone, and with 5 μg/mL LPS significantly increased the ZO-1 intensity at EC junctions. In the presence of TCs (Fig. 5B), pretreatments of cAMP also enhanced ZO-1 intensity at the EC junctions without TCs (w/o TCs) and with adherent TCs (AD) compared to those without cAMP treatment (Fig. 3G). Consequently, cAMP reduced P of EC monolayers from the control and decreased the enhanced P by LPS in the absence (Fig. 5C) and presence of

TCs (Fig. 5D). cAMP also reduced TC transmigration from the control and completely abolished the increased TC transmigration by LPS (Fig. 5E).

We also examined the effects of cAMP, VEGF and LPS on endothelial surface glycocalyx (ESG). After 2 h cAMP treatment, no significant change in the ESG was observed compared with the control. In contrast, after 1 h treatment with VEGF and LPS, ESG was degraded by more than 60% and 90%, respectively.

Discussion

Using an in vitro microvessel wall model and high resolution confocal microscopy, we were able to quantify the transmigration locations of MDA-MB-231 across brain (bEnd3) and lung (RLMEC) microvascular endothelial barriers, two preferential sites for breast cancer metastases. To ensure the confluence of endothelial monolayers, in addition to continuous labeling of EC junction protein ZO-1, we measured the permeability of monolayers to albumin and compare it with in vivo data. The permeability of bEnd3 monolayers to albumin is 1.2×10^{-7} cm/s, which is comparable to permeability of the similar sized Dextran-70k, 1.1×10^{-7} cm/s, measured in rat cerebral microvessels in vivo [49]. The permeability of RLMEC monolayers to albumin is 8.5×10^{-7} cm/s, comparable to what measured in rat mesenteric microvessels in vivo, 8.1×10^{-7} cm/s [8]. After confluence, TCs were added into the upper chamber of the trans-well filter. We found that for both EC monolayers, 98% of TC transmigration occurred at the inter-endothelial junctions, only 2% through cell bodies. Out of 98%, about 2/3 through the tri-cellular joints. These observations are consistent with study by Burns et al. [7] for the neutrophil migration across HUVEC monolayers, suggesting a similar mechanism by which TCs and leukocytes accomplish their transmigration across microvessel walls. These results are also consistent with our previous study on TC adhesion to bEnd3 monolayers [19], suggesting that adhesion is the initial step for TC extravasation [30, 37, 60].

To investigate how TCs transmigrate through the EC barrier, we quantified endothelial surface glycocalyx (ESG) and EC junction protein, ZO-1, during adhesion and transmigrating. Our results showed that more than 60% of ESG was degraded after 1 h TC incubation, ZO-1 was partially disrupted during 4-8 h adhesion and completely disrupted during transmigrating. After TC transmigration, we did see some ZO-1 in the vicinity of transmigrated TCs (Fig. 2E). This implies that EC junctions can be resealed after TC transmigration, as observed in Chen et al. [10]. In addition to disrupting the tight junction ZO-1 during TC adhesion and transmigration as shown in the current study, others reported dislocation and disruption of the adherens junction VE-cadherin between ECs during these processes [10, 19, 29, 32, 35, 58]. Together these findings suggested that TCs prefer to adhere and transmigrate through the EC joints instead of bodies for undamaged ECs.

To test whether degradation of ESG increases TC adhesion, and also to confirm that the observed reduction in the ESG during TC adhesion and transmigration was not due to the redistribution of the glycocalyx, we used 50 mU/mL heparinase III to pretreat the bEnd3 monolayers for 1 h before adding the TCs. Figure 6 demonstrates our results. The intensity of AF488-anti-HS reduced to ~42% of that for the control (Figs. 6A, B, E), and the number

of the adherent TCs increased by ~2.5 fold after 1 h adhesion (Figs. 6C, D, E). Degradation of the ESG may expose more adhesion molecules of the ECs to TCs to increase their adhesion as suggested by Schmidt et al.[46] for neutrophil adhesion.

While ESG and EC junction proteins represent local endothelial integrity, the endothelial permeability reflects EC integrity in a global sense. We thus quantified endothelial permeability to albumin P under various conditions. After 4 h incubation with TCs at a seeding density of 600 cells/mm^2, 555 and 417 cells/mm^2 adhered, transmigrating and transmigrated across bEnd3 and RLMEC monolayers, respectively. With about 7 fold higher P under control, the RLMEC monolayer attracts 33% more TCs than the bEnd3 monolayer at 4h, but 3 fold higher in effective transmigrated TCs. The higher EC permeability does correlate with the higher TC transmigration. The observation by Jeon et al.[32] that the leakiest environment of an in vitro EC channel gave rise to the lowest TC extravasation rate implies additional contributions from the basement membrane and the surrounding tissue. Interestingly, we found a same TC effective transmigrated rate, ~25 cells/mm^2/h, during 4-8 h, for bEnd3 and RLMEC monolayers with much different P. Correspondingly, TC transmigration greatly enhanced P. The relative increasing rate, $(P_{with\ TC} - P_{without\ TC})/P_{without\ TC}$ was about 50%/h for both EC monolayers during 4-8h incubation. The highly enhanced P due to TC transmigration may allow the passage of water and other molecules in the blood into tissues, causing damages in addition to tumor metastasis.

Under pathological conditions such as inflammation and influence by TC secretion, the EC integrity was comprised by LPS and VEGF, resulting in increased EC P and TC transmigration. Our results demonstrated that the effect of TC transmigration on P was overwhelmingly larger than that of 1 nM VEGF and 5 μg/mL LPS, which are typical concentrations of local TC secretion [19, 48] and systemic inflammation [25], especially at longer time, suggesting that even without other pathological influences, TC transmigration alone can significantly disrupt EC integrity. However, with the help of VEGF and LPS, TC can enhance their transmigration efficiency by 1.5-5 fold at different timing for bEnd3 and RLMEC monolayers, indicating activating effects of VEGF and LPS on TCs and ECs in addition to increasing P of EC monolayers. The mechanisms by which LPS and VEGF diminish the ESG are not quite clear. LPS can degrade the ESG by a heparanase mediated mechanism [46]. Via activation of endothelial receptors, followed by fluxes of calcium ions, nucleotides, phospholipids, and ionic second messengers, VEGF can induce cytoskeleton tension [4] and might indirectly affect the trans-membrane ESG core proteins such as syndecans and diminish the ESG. Further investigation is necessary to elucidate the mechanisms.

Using a parallel-plate flow chamber, Chotard-Ghodsnia et al. [12] investigated TC and EC interactions under shear flow. They found that although the blood shear flow affected TC adhesion to the EC monolayer, the transmigration was independent of the shear flow. Similar results were observed for leukocyte extravasation [13]. From these previous studies, we anticipated that our current results for TC transmigration under static conditions are also valid under shear flow.

Finally, by using cAMP to reinforce endothelial integrity, especially the EC junctions [1, 15, 23, 45], we could successfully prevent TC transmigration and increase in endothelial permeability. In conclusion, quantifying where, how and how fast TCs transmigrate across EC barriers is the first step to uncover the mechanisms by which tumor cells accomplish their extravasation and to find an efficient way to inhibit this process.

Acknowledgements

References

1. Adamson RH, Ly JC, Sarai RK, Lenz JF, Altangerel A, Drenckhahn D, Curry FE. Epac/Rap1 pathway regulates microvascular hyperpermeability induced by PAF in rat mesentery. Am J Physiol Heart Circ Physiol. 2008; 294:H1188–1196. [PubMed: 18178724]

2. Al-Mehdi AB, Tozawa K, Fisher AB, Shientag L, Lee A, Muschel RJ. Intravascular origin of metastasis from the proliferation of endothelium-attached tumor cells: a new model for metastasis. Nat Med. 2000; 6:100–102. [PubMed: 10613833]

3. Arvanitis C, Khuon S, Spann R, Ridge KM, Chew TL. Structure and biomechanics of the endothelial transcellular circumferential invasion array in tumor invasion. PLoS One. 2014; 9:e89758. [PubMed: 24587014]

4. Bates DO. Vascular endothelial growth factors and vascular permeability. Cardiovasc Res. 2010; 87:262–271. [PubMed: 20400620]

5. Bendas G, Borsig L. Cancer cell adhesion and metastasis: selectins, integrins, and the inhibitory potential of heparins. Int J Cell Biol. 2012; 2012:676731. [PubMed: 22505933]

6. Brenner W, Langer P, Oesch F, Edgell CJ, Wieser RJ. Tumor cell--endothelium adhesion in an artificial venule. Anal Biochem. 1995; 225:213–219. [PubMed: 7762783]

7. Burns AR, Walker DC, Brown ES, Thurmon LT, Bowden RA, Keese CR, Simon SI, Entman ML, Smith CW. Neutrophil transendothelial migration is independent of tight junctions and occurs preferentially at tricellular corners. J Immunol. 1997; 159:2893–2903. [PubMed: 9300713]

8. Cai B, Fan J, Zeng M, Zhang L, Fu BM. Adhesion of malignant mammary tumor cells MDA-MB-231 to microvessel wall increases microvascular permeability via degradation of endothelial surface glycocalyx. J Appl Physiol. 2012; 113:1141–1153. [PubMed: 22858626]

9. Chen C, Khismatullin DB. Lipopolysaccharide induces the interactions of breast cancer and endothelial cells via activated monocytes. Cancer Lett. 2014; 345:75–84. [PubMed: 24333719]

10. Chen MB, Whisler JA, Jeon JS, Kamm RD. Mechanisms of tumor cell extravasation in an in vitro microvascular network platform. Integr Biol (Camb). 2013; 5:1262–1271. [PubMed: 23995847]

11. Cheung LS, Raman PS, Balzer EM, Wirtz D, Konstantopoulos K. Biophysics of selectin-ligand interactions in inflammation and cancer. Phys Biol. 2011; 8:015013. [PubMed: 21301059]

12. Chotard-Ghodsnia R, Haddad O, Leyrat A, Drochon A, Verdier C, Duperray A. Morphological analysis of tumor cell/endothelial cell interactions under shear flow. J Biomech. 2007; 40:335–344. [PubMed: 16497312]

13. Cinamon G, Alon R. A real time in vitro assay for studying leukocyte transendothelial migration under physiological flow conditions. J Immunol Methods. 2003; 273:53–62. [PubMed: 12535797]

14. Constantinescu AA, Vink H, Spaan JA. Endothelial cell glycocalyx modulates immobilization of leukocytes at the endothelial surface. Arterioscler Thromb Vasc Biol. 2003; 23:1541–1547. [PubMed: 12855481]

15. Curry FR, Adamson RH. Vascular permeability modulation at the cell, microvessel, or whole organ level: towards closing gaps in our knowledge. Cardiovasc Res. 2010; 87:218–229. [PubMed: 20418473]

16. Curry FR, Noll T. Spotlight on microvascular permeability. Cardiovasc Res. 2010; 87:195–197. [PubMed: 20542875]

17. Earley S, Plopper GE. Disruption of focal adhesion kinase slows transendothelial migration of AU-565 breast cancer cells. Biochem Biophys Res Commun. 2006; 350:405–412. [PubMed: 17010315]

18. Eichler AF, Chung E, Kodack DP, Loeffler JS, Fukumura D, Jain RK. The biology of brain metastases-translation to new therapies. Nat Rev Clin Oncol. 2011; 8:344–356. [PubMed: 21487419]

19. Fan J, Cai B, Zeng M, Hao Y, Giancotti FG, Fu BM. Integrin beta4 signaling promotes mammary tumor cell adhesion to brain microvascular endothelium by inducing ErbB2-mediated secretion of VEGF. Ann Biomed Eng. 2011; 39:2223–2241. [PubMed: 21556948]

20. Fazakas C, Wilhelm I, Nagyoszi P, Farkas AE, Hasko J, Molnar J, Bauer H, Bauer HC, Ayaydin F, Dung NT, Siklos L, Krizbai IA. Transmigration of melanoma cells through the blood-brain barrier: role of endothelial tight junctions and melanoma-released serine proteases. PLoS One. 2011; 6:e20758. [PubMed: 21674054]

21. Fertig EJ, Lee E, Pandey NB, Popel AS. Analysis of gene expression of secreted factors associated with breast cancer metastases in breast cancer subtypes. Sci Rep. 2015; 5:12133. [PubMed: 26173622]

22. Fidler IJ. The pathogenesis of cancer metastasis: the 'seed and soil' hypothesis revisited. Nat Rev Cancer. 2003; 3:453–458. [PubMed: 12778135]

23. Fu BM, Shen S, Chen B. Structural mechanisms in the abolishment of VEGF-induced microvascular hyperpermeability by cAMP. J Biomech Eng. 2006; 128:317–328. [PubMed: 16706581]

24. Fu BM, Tarbell JM. Mechano-sensing and transduction by endothelial surface glycocalyx: composition, structure, and function. Wiley Interdiscip Rev Syst Biol Med. 2013; 5:381–390. [PubMed: 23401243]

25. Ghaly T, Rabadi MM, Weber M, Rabadi SM, Bank M, Grom JM, Fallon JT, Goligorsky MS, Ratliff BB. Hydrogel-embedded endothelial progenitor cells evade LPS and mitigate endotoxemia. Am J Physiol Renal Physiol. 2011; 301:F802–812. [PubMed: 21775481]

26. Glinskii OV, Huxley VH, Glinsky GV, Pienta KJ, Raz A, Glinsky VV. Mechanical entrapment is insufficient and intercellular adhesion is essential for metastatic cell arrest in distant organs. Neoplasia. 2005; 7:522–527. [PubMed: 15967104]

27. Glinskii OV, Li F, Wilson LS, Barnes S, Rittenhouse-Olson K, Barchi JJ Jr. Pienta KJ, Glinsky VV. Endothelial integrin alpha3beta1 stabilizes carbohydrate-mediated tumor/endothelial cell adhesion and induces macromolecular signaling complex formation at the endothelial cell membrane. Oncotarget. 2014; 5:1382–1389. [PubMed: 24675526]

28. Haddad O, Chotard-Ghodsnia R, Verdier C, Duperray A. Tumor cell/endothelial cell tight contact upregulates endothelial adhesion molecule expression mediated by NFkappaB: differential role of the shear stress. Exp Cell Res. 2010; 316:615–626. [PubMed: 19944683]

29. Hamilla SM, Stroka KM, Aranda-Espinoza H. VE-cadherin-independent cancer cell incorporation into the vascular endothelium precedes transmigration. PLoS One. 2014; 9:e109748. [PubMed: 25275457]

30. Heyder C, Gloria-Maercker E, Entschladen F, Hatzmann W, Niggemann B, Zanker KS, Dittmar T. Realtime visualization of tumor cell/endothelial cell interactions during transmigration across the endothelial barrier. J Cancer Res Clin Oncol. 2002; 128:533–538. [PubMed: 12384796]

31. Heyder C, Gloria-Maercker E, Hatzmann W, Zaenker KS, Dittmar T. Visualization of tumor cell extravasation. Contributions to microbiology. 2006; 13:200–208. [PubMed: 16627967]

32. Jeon JS, Bersini S, Gilardi M, Dubini G, Charest JL, Moretti M, Kamm RD. Human 3D vascularized organotypic microfluidic assays to study breast cancer cell extravasation. Proc Natl Acad Sci U S A. 2015; 112:214–219. [PubMed: 25524628]

33. Kienast Y, von Baumgarten L, Fuhrmann M, Klinkert WE, Goldbrunner R, Herms J, Winkler F. Real-time imaging reveals the single steps of brain metastasis formation. Nat Med. 2010; 16:116–122. [PubMed: 20023634]

34. Kuperwasser C, Dessain S, Bierbaum BE, Garnet D, Sperandio K, Gauvin GP, Naber SP, Weinberg RA, Rosenblatt M. A mouse model of human breast cancer metastasis to human bone. Cancer Res. 2005; 65:6130–6138. [PubMed: 16024614]

35. Lee TH, Avraham HK, Jiang S, Avraham S. Vascular endothelial growth factor modulates the transendothelial migration of MDA-MB-231 breast cancer cells through regulation of brain microvascular endothelial cell permeability. J Biol Chem. 2003; 278:5277–5284. [PubMed: 12446667]

36. Li G, Simon MJ, Cancel LM, Shi ZD, Ji X, Tarbell JM, Morrison B 3rd, Fu BM. Permeability of endothelial and astrocyte cocultures: in vitro blood-brain barrier models for drug delivery studies. Ann Biomed Eng. 2010; 38:2499–2511. [PubMed: 20361260]

37. Miles FL, Pruitt FL, van Golen KL, Cooper CR. Stepping out of the flow: capillary extravasation in cancer metastasis. Clin Exp Metastasis. 2008; 25:305–324. [PubMed: 17906932]

38. Mulivor AW, Lipowsky HH. Inhibition of glycan shedding and leukocyte endothelial adhesion in postcapillary venules by suppression of matrixmetalloprotease activity with doxycycline. Microcirculation. 2009; 16:657–666. [PubMed: 19905966]

39. Muller A, Homey B, Soto H, Ge N, Catron D, Buchanan ME, McClanahan T, Murphy E, Yuan W, Wagner SN, Barrera JL, Mohar A, Verastegui E, Zlotnik A. Involvement of chemokine receptors in breast cancer metastasis. Nature. 2001; 410:50–56. [PubMed: 11242036]

40. Nguyen DX, Bos PD, Massague J. Metastasis: from dissemination to organ-specific colonization. Nat Rev Cancer. 2009; 9:274–284. [PubMed: 19308067]

41. Peyssonnaux C, Cejudo-Martin P, Doedens A, Zinkernagel AS, Johnson RS, Nizet V. Cutting edge: Essential role of hypoxia inducible factor-1alpha in development of lipopolysaccharide-induced sepsis. J Immunol. 2007; 178:7516–7519. [PubMed: 17548584]

42. Pries AR, Secomb TW, Gaehtgens P. The endothelial surface layer. Pflugers Arch. 2000; 440:653–666. [PubMed: 11007304]

43. Reitsma S, Slaaf DW, Vink H, van Zandvoort MA, Egbrink M. G. oude. The endothelial glycocalyx: composition, functions, and visualization. Pflugers Arch. 2007; 454:345–359. [PubMed: 17256154]

44. Schick MA, Wunder C, Wollborn J, Roewer N, Waschke J, Germer CT, Schlegel N. Phosphodiesterase-4 inhibition as a therapeutic approach to treat capillary leakage in systemic inflammation. J Physiol. 2012; 590:2693–2708. [PubMed: 22495586]

45. Schlegel N, Waschke J. cAMP with other signaling cues converges on Rac1 to stabilize the endothelial barrier- a signaling pathway compromised in inflammation. Cell Tissue Res. 2014; 355:587–596. [PubMed: 24322391]

46. Schmidt EP, Yang Y, Janssen WJ, Gandjeva A, Perez MJ, Barthel L, Zemans RL, Bowman JC, Koyanagi DE, Yunt ZX, Smith LP, Cheng SS, Overdier KH, Thompson KR, Geraci MW, Douglas IS, Pearse DB, Tuder RM. The pulmonary endothelial glycocalyx regulates neutrophil adhesion and lung injury during experimental sepsis. Nat Med. 2012; 18:1217–1223. [PubMed: 22820644]

47. Schumacher D, Strilic B, Sivaraj KK, Wettschureck N, Offermanns S. Platelet-derived nucleotides promote tumor-cell transendothelial migration and metastasis via P2Y2 receptor. Cancer Cell. 2013; 24:130–137. [PubMed: 23810565]

48. Shen S, Fan J, Cai B, Lv Y, Zeng M, Hao Y, Giancotti FG, Fu BM. Vascular endothelial growth factor enhances cancer cell adhesion to microvascular endothelium in vivo. Exp Physiol. 2010; 95:369–379. [PubMed: 19880535]

49. Shi L, Zeng M, Sun Y, Fu BM. Quantification of blood-brain barrier solute permeability and brain transport by multiphoton microscopy. J Biomech Eng. 2014; 136:031005. [PubMed: 24193698]

50. Slattery MJ, Liang S, Dong C. Distinct role of hydrodynamic shear in leukocyte-facilitated tumor cell extravasation. Am J Physiol Cell Physiol. 2005; 288:C831–839. [PubMed: 15601752]

51. Steeg PS. Tumor metastasis: mechanistic insights and clinical challenges. Nat Med. 2006; 12:895–904. [PubMed: 16892035]

52. Stoletov K, Kato H, Zardouzian E, Kelber J, Yang J, Shattil S, Klemke R. Visualizing extravasation dynamics of metastatic tumor cells. J Cell Sci. 2010; 123:2332–2341. [PubMed: 20530574]

53. Tarbell JM, Pahakis MY. Mechanotransduction and the glycocalyx. J Intern Med. 2006; 259:339–350. [PubMed: 16594902]

54. Thorley AJ, Giembycz MA, Goldstraw P, Young A, Tetley TD. Differential regulation of cytokine release and leukocyte migration by lipopolysaccharide-stimulated primary human lung alveolar type II epithelial cells and macrophages. J Immunol. 2007; 178:463–473. [PubMed: 17182585]

55. Tremblay PL, Auger FA, Huot J. Regulation of transendothelial migration of colon cancer cells by E-selectin-mediated activation of p38 and ERK MAP kinases. Oncogene. 2006; 25:6563–6573. [PubMed: 16715142]

56. Tremblay PL, Huot J, Auger FA. Mechanisms by which E-selectin regulates diapedesis of colon cancer cells under flow conditions. Cancer Res. 2008; 68:5167–5176. [PubMed: 18593916]

57. Vlodavsky I, Elkin M, Abboud-Jarrous G, Levi-Adam F, Fuks L, Shafat I, Ilan N. Heparanase: one molecule with multiple functions in cancer progression. Connect Tissue Res. 2008; 49:207–210. [PubMed: 18661344]

58. Weidert E, Pohler SE, Gomez EW, Dong C. Actinomyosin contraction, phosphorylation of VE-cadherin, and actin remodeling enable melanoma-induced endothelial cell-cell junction disassembly. PLoS One. 2014; 9:e108092. [PubMed: 25225982]

59. Weis S, Cui J, Barnes L, Cheresh D. Endothelial barrier disruption by VEGF-mediated Src activity potentiates tumor cell extravasation and metastasis. J Cell Biol. 2004; 167:223–229. [PubMed: 15504909]

60. Zen K, Liu DQ, Guo YL, Wang C, Shan J, Fang M, Zhang CY, Liu Y. CD44v4 is a major E-selectin ligand that mediates breast cancer cell transendothelial migration. PLoS One. 2008; 3:e1826. [PubMed: 18350162]
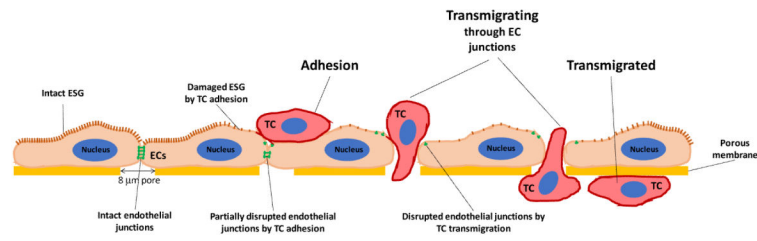
Fig. 1.
Schematic showing tumor cell transmigration process (adhesion, transmigrating and transmigrated) across an endothelial monolayer (an in vitro model for the microvessel wall) and hypothetic mechanisms by which tumor cell adhesion and transmigration compromise endothelial integrity by degrading endothelial surface glycocalyx (ESG) and disrupting endothelial junctions.
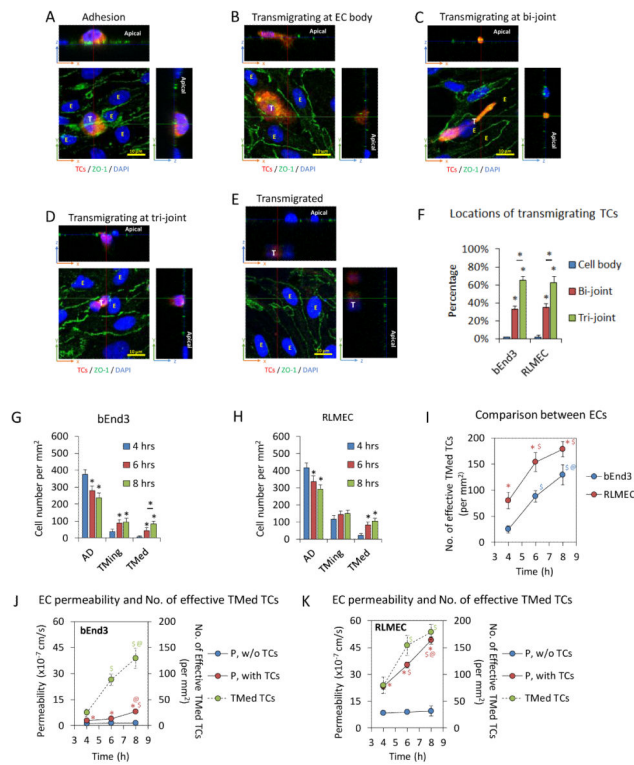
Fig. 2.
Tumor cell (TC) transmigration locations, transmigration rates and corresponding permeability of endothelial cell (EC) monolayers to BSA. Confocal images showing TC (red) adhesion to EC junctions (ZO-1, green) **(A)**, TC transmigrating at the EC body (nucleus, blue) **(B)**, at the joint between two ECs (bi-joint) **(C),** at the joint between three ECs (tri-joint) **(D)** and TC transmigrated to the basal side of an EC monolayer **(E)**. Summary of locations of total transmigrating TCs across bEnd3 (mouse brain microvessel endothelial cell) and RLMEC (rat lung microvessel endothelial cell) monolayers out of 9 samples (3 samples each at 4, 6, and 8h) for each EC **(F)**. * $p < 0.05$. Values are means ± SE. Numbers of adherent, transmigrating and transmigrated TCs at 4, 6, and 8h on/across bEnd3 **(G)** and RLMEC **(H)** monolayers. * $p < 0.05$. Values are means ± SE. Comparison of the number of effective transmigrated TCs across bEnd3 and RLMEC monolayers at 4, 6 and 8 h **(I)**. The number of effective transmigrated TCs = the number of transmigrated TCs + 0.5 × the number of transmigrating TCs. * $p < 0.05$, comparison between different EC monolayers at the same time. $ $p < 0.05$, comparison between 6 h or 8 h with 4 h; @ $p < 0.05$, comparison between 8 h and 6 h, for each EC monolayer. Values are means ± SE. Comparison of the number of effective transmigrated TCs (green filled circles) and the permeability to BSA (red filled circles) at 4, 6 and 8 h for bEnd3 **(J)** and RLMEC **(K)** monolayers. The permeability of the control group without adding TCs is plotted with the blue filled circles for each EC monolayer. * $p < 0.05$, compared with the control permeability at the same time; $ $p < 0.05$, comparison between 6 h or 8 h with 4 h; @ $p < 0.05$, comparison between 8h and 6h, for each EC monolayer. Values are means ± SE. For all the measurements, n = 3 samples at each time for each EC.
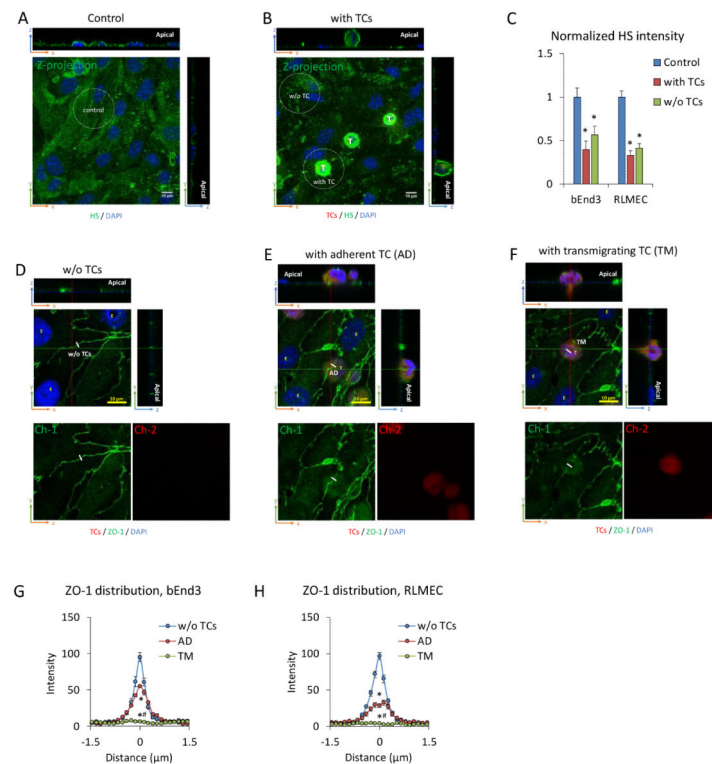
Fig. 3.

Tumor cell adhesion and transmigration degrade endothelial surface glycocalyx (ESG) and disrupt endothelial junction proteins (ZO-1). Confocal images showing AF488-anti-HS labeled ESG (green) on RLMEC monolayers under control (**A**) and after 1h TC adhesion (**B**). "T" in (**B**) with the bright green color are tumor cells having abundant HS. Comparison of the intensity of AF488-anti-HS labeled ESG in EC regions with adherent TCs and those without for bEnd3 and RLMEC monolayers (**C**). The average intensity of AF488-anti-HS on 10-15 EC regions of interest (ROIs) with adherent TCs and those without adherent TCs in the same sample are normalized by the average intensity of AF488-anti-HS on 10-15 ROIs from the control sample without adding TCs. A ROI with an adherent TC is defined as the white dotted line circled region having a diameter of 3 TCs and with a TC in the middle. The intensity of AF488-anti-HS in a ROI with an adherent TC = the total intensity of the circled area - the intensity of AF488-anti-HS on the TC. The intensity of AF488-anti-HS in a ROI without TCs is the total intensity of the circled area, which is at least 2 TCs far from the ROIs with adherent TCs. * $p < 0.05$, compared with the control. n= 3, Values are means ± SE. Confocal images showing AF488-anti-ZO-1 labeled EC junctions (green) without TCs (**D**), with an adherent TC (AD) (**E**) and with a transmigrating TC (TM) (**F**). Tumor cells are labeled in red and nuclei of ECs and TCs are labeled with DAPI (blue). Top images are merged images and the images in the bottom left (Ch-1) show ZO-1 labeling only (green) and those in the bottom right (Ch-2) show tumor cells only (red). Comparison of the intensity profiles of ZO-1 labeling along a 3 μm line perpendicular to the EC junctions (white line in **D-F**) for the EC junctions without TCs (blue line with circles), with adherent TCs (AD) (red line with circles) and with transmigrating TCs (TM) (green line with circles) for bEnd3 (**G**) and RLMEC (**H**) monolayers. For each sample, 15-60 measured profiles from

5-20 EC pairs for each case. n = 3 samples at each time point. Values are means ± SE. Since there are no significant difference between 4, 6 and 8 h for each case, the intensity shown here is the average over these 3 time points. Kurtosis analysis indicates that the intensity profiles of ZO-1 are significantly different for the EC junctions without TCs, with adherent TCs and with transmigrating TCs. * $p < 0.05$, compared with no TCs; # $p < 0.05$, TM compared with AD.
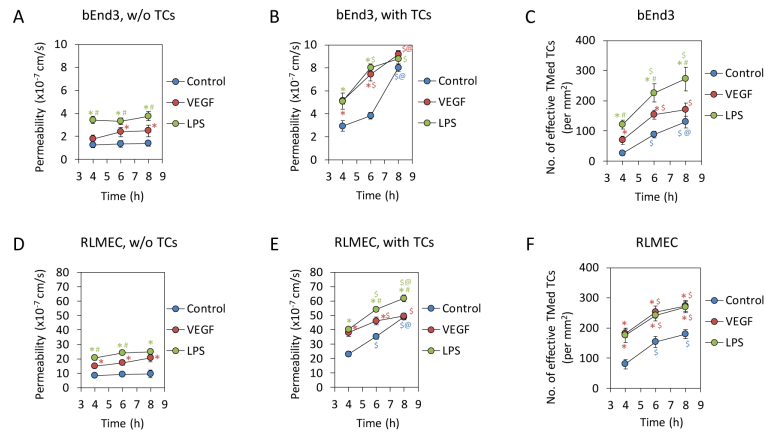
Fig. 4.
Effects of VEGF and LPS on permeability of EC monolayers to BSA and on tumor cell transmigration. Comparison of permeability of EC monolayers to BSA under control and under 1 nM VEGF or 5 μg/mL LPS treatment in the absence (**A, D**) and presence of tumor cells (**B, E**) for bEnd3 and RLMEC monolayers, respectively. Comparison of the number of effective transmigrated tumor cells (TMed TCs) across EC monolayers under control and under 1 nM VEGF or 5 μg/mL LPS treatment for bEnd3 (**C**) and RLMEC (**F**). * $p < 0.05$, compared with control at the same time; # $p < 0.05$, compare VEGF treatment with LPS treatment at the same time; $^\$$ $p < 0.05$, compare 6h or 8h with 4h under same treatments; @ $p < 0.05$, compare 8h with 6h under same treatments. n = 3 for each time point. Values are means ± SE.
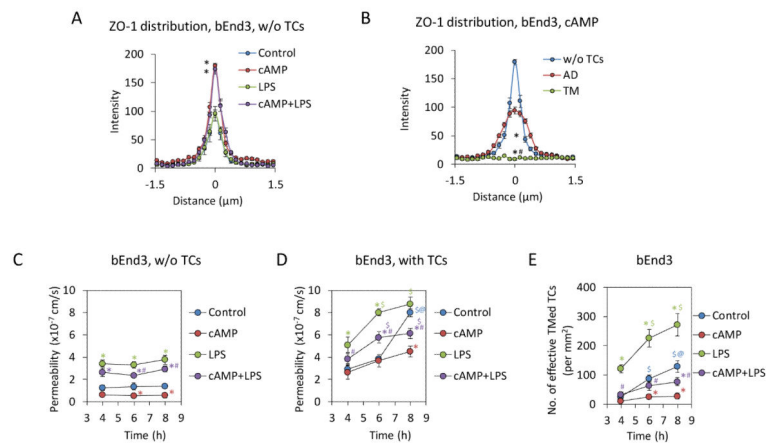
Fig. 5.

Effects of cAMP on bEnd3 endothelial junctions, tumor cell transmigration and endothelial permeability to BSA. Comparison of the intensity profiles of ZO-1 labeling along a 3 μm line perpendicular to the EC junctions (white line in Fig. 3D-F) for the EC junctions under control without adding TCs, after 2h 4mM cAMP pretreatment and add TCs, TCs with 5μg/mL LPS, pretreatment of 4 mM cAMP for 2h, then with 4 mM cAMP + 5μg/mL LPS (**A**). The intensity profile for each case is the averaged profile over 4, 6 and 8 h after TC incubation at the locations without TCs (see Fig. 3D). For each sample, 60 measured profiles from 20 EC pairs. n = 3 samples for each case at each time. Values are means ± SE. * p < 0.05 compared with the control based on the Kurtosis analysis. Comparison of the intensity profiles of ZO-1 labeling along a 3 μm line perpendicular to the EC junctions for the EC junctions without TCs, with adherent TCs (AD) and with transmigrating TCs (TM) after 2 h pretreatment with 4 mM cAMP and incubation with TCs (**B**). For each sample, 9-60 measured profiles from 3-20 EC pairs for each case. n = 3 samples at each time point. Values are means ± SE. Since there are no significant difference between 4, 6 and 8 h for each case, the intensity shown here is the average over these 3 time points. Kurtosis analysis indicates that the intensity profiles of ZO-1 are significantly different for these three cases. * p < 0.05, compared with no TCs; [#] p < 0.05, TM compared with AD. Comparison of permeability of bEnd3 monolayers to BSA in the absence (**C**) and presence of tumor cells (**D**) and the number of effective transmigrated tumor cells (TMed TCs) across bEnd3 monolayers (**E**) under control and under cAMP, LPS and cAMP + LPS treatments. * p < 0.05, compared with control at the same time; # p < 0.05, compare cAMP treatment with cAMP + LPS treatment at the same time; [$] p < 0.05, compare 6h or 8h with 4h under same treatments; [@] p < 0.05, compare 8h with 6h under same treatments. n = 3 for each time point. Values are means ± SE.
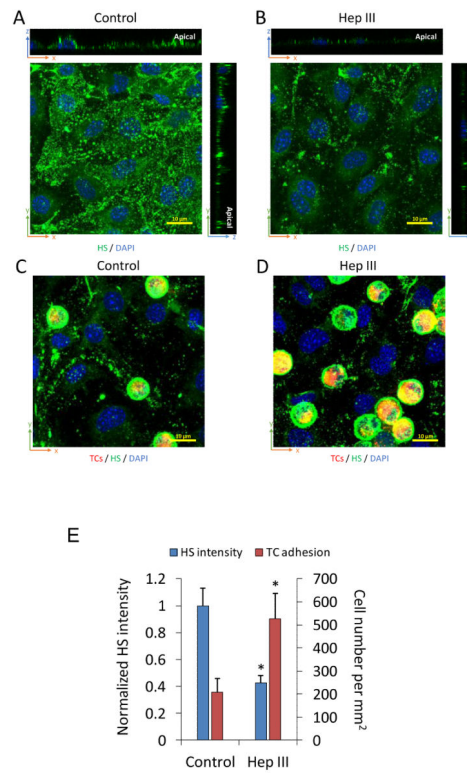
Fig. 6.
Effects of heparinase on ESG of EC monolayers and tumor cell adhesion. Confocal images showing AF488-anti-HS labeled ESG (green) on bEnd3 monolayers under control (**A**) and after 1 h 50 mU/mL heparinase III pretreatment (**B**). 1 h tumor cell adhesion under control (**C**) and that after 1 h heparinase III pretreatment (**D**). Comparison of the intensity of AF488-anti-HS labeled ESG on bEnd3 monolayers and the number of adherent tumor cells under control and after 1 h heparinase pretreatment (**E**). * $p < 0.05$, compared with the control. n = 3, Values are means ± SE.